Angle-differential and momentum-transfer cross sections for low-energy electron-Cs scattering

U. Thumm† and D. W. Norcross*
Joint Institute for Laboratory Astrophysics, University of Colorado, Boulder, Colorado 80309-0440 and National Institute of Standards and Technology, Boulder, Colorado 80309-0440
(Received 23 July 1992)

Based on a previous Dirac R-matrix calculation [U. Thumm and D. W. Norcross, Phys. Rev. A **45**, 6349 (1992)], we have derived elastic and inelastic angle-differential and elastic momentum-transfer cross sections for slow electrons ($E_{\rm kin} \leq 2.8$ eV) colliding with neutral Cs atoms. Our results for the angle-differential cross sections are in good agreement with scaled experimental data and, depending on the incident electron energy, in qualitative or fair quantitative agreement with previously published theoretical work. The inelastic angle-differential cross sections for $6p_{1/2}$ and $6p_{3/2}$ excitation differ by more than a statistical branching ratio due to relativistic effects. For the momentum-transfer cross sections, we hope to resolve existing discrepancies in the literature and to provide more reliable input for transport calculations.

PACS number(s): 34.80.Bm, 31.20.Tz, 31.30.Jv, 34.80.Dp

I. INTRODUCTION

There is a rather substantial body of work on slow collisions of electrons with alkali-metal atoms, in particular with cesium [1–16]. While for light target atoms such as hydrogen, lithium, sodium, and potassium, calculations are usually based on the Schrödinger equation and may include relativistic effects in a weak relativistic approximation through spin-orbital angular-momentum-coupling potentials [7, 9, 10], such an approach is questionable for heavier elements such as rubidium, cesium, and francium. For these heavier alkali-metal atoms, relativistic effects on their electronic structure are apparent, e.g., through large fine-structure splittings, and are also expected to be of importance for the detailed interaction between the heavy atom and the scattering electron. In particular, the large fine-structure splitting of the heavy neutral target has a direct counterpart in multiplets of negative-ion resonances formed during the electron impact, with fine-structure splittings that may by far exceed the autoionization widths of the individual terms [12].

For cesium targets and slow incident electrons (by "slow" we mean kinetic energies of the projectile below the first atomic-ionization threshold), several calculations are available [1–3, 5–7, 9, 10, 12]. However, only a few theoretical approaches take relativistic corrections into account in a nonperturbative way [1, 6, 12], either by starting from the Dirac equation [1,12] or by using a geometrical LS-jj recoupling transformation [6] of an otherwise nonrelativistic theory. On the experimental side, only a few papers with reliable results have been published [4, 8, 11, 13] and the agreement of (low-resolution) absolute total cross sections [4, 11] with recent theoretical predictions [1, 12] is at the 10–20 % level at most measured incident electron energies and at some energies is much worse.

Low-lying $6s6p\,^3P^o$, $6p^2\,^3P^e$, and $6p5d\,^3F^o$ resonances in the electron-cesium scattering system are of considerable interest and are the subject of controversy in the literature, as we have outlined before [1, 12]. In a recently published relativistic R-matrix calculation [1], we have identified the $^3P^e$ and $^3P^o$ resonances in partial and total angle-integrated scattering cross sections. The existence of a $^3F^o$ resonance has been proposed before in an earlier close-coupling calculation [3, 6] and in the measurement of angle-differential cross sections [8]. In the present paper, we direct our attention to angle-differential and momentum-transfer cross sections, which both depend more sensitively on the detailed dynamics of the scattering process than total angle-integrated cross sections.

Momentum-transfer cross sections for scattered electrons with 0.1 to 1 eV kinetic energy are of particular technological interest for the development of thermionic converters [17]. So far, at these low energies, electron-cesium momentum-transfer cross sections have been extracted from swarm experiments [14–16] (e.g., through measured electrical or thermal conductivities) and from the measured collisional broadening of cesium Rydberg states [13]. These rather indirect methods of determining momentum-transfer cross sections are in general difficult to perform, and it is therefore not surprising that previously published results [13–16] are contradictory. Our relativistic close-coupling ansatz allows for the *direct* calculation of momentum-transfer cross sections, even for the lowest scattering energies, and thus circumvents difficulties associated with the inversion of transport equations and the deconvolution of cross sections and electron-velocity distributions.

We organized this paper as follows. Section II gives a brief summary of the Dirac R-matrix calculation that underlies this work. Our results for angle-differential and momentum-transfer cross sections are presented and discussed in Sec. III. We also briefly revisit, in the light

of recent measurements [11], our earlier reports [1, 12] on total integrated cross sections. Section IV contains a summary and conclusions. In the Appendix, we derive the spin-dependent scattering amplitude as a function of the K matrices, which constitutes the link between the results presented in this paper and those previously published [1]. Unless otherwise stated, we use atomic units of length (a_0), area (πa_0^2), and polarizability (a_0^3), with the Bohr radius $a_0 = 5.292 \times 10^{-11}$ m.

II. METHOD OF CALCULATION

We have recently applied the Dirac R-matrix method to the calculation of negative-ion binding energies and elastic and inelastic total-scattering cross sections for electrons colliding with neutral cesium at kinetic energies up to 2.8 eV [1, 12]. The calculation is built upon a two-electron model for the electron-cesium scattering system. In this model, the two active electrons (the scattered electron and the valence electron of the target) interact with the noble-gas-like core of the target through semiempirical Thomas-Fermi-type and core-polarization potentials. The adjustable parameters in these ℓ- and j-dependent potentials are determined by fitting [18] calculated energies of neutral cesium to the most reliable available experimental energies. The interaction between the two active electrons contains the usual Coulomb interaction and an additional core-polarization potential, the so-called dielectronic term, which we adjust to the measured electron affinity of Cs. The scattering calculation includes close coupling between the $6s_{1/2}\,^2S_{1/2}$, $6p_{1/2}\,^2P_{1/2}$, $6p_{3/2}\,^2P_{3/2}$, $5d_{3/2}\,^2D_{3/2}$, and $5d_{5/2}\,^2D_{5/2}$ states of the target. We use 24 continuum orbitals in each scattering channel and include a Buttle correction to correct for incompleteness in the basis of continuum orbitals. The continuum orbitals satisfy relativistic R-matrix boundary conditions and are jj coupled to bound valence orbitals, which leads to a set of two-electron wave functions in each J^π scattering symmetry (J and π are the total angular momentum and parity of the scattering system).

In addition to these functions, we also include a variable number of two-electron bound states in order to obtain a basis of two-electron wave functions with respect to which we diagonalize the total Hamiltonian of the two-electron model system. This diagonalization includes electron exchange and all one-electron relativistic effects. It is restricted in space to the inner region of the R-matrix calculation, given by a sphere of radius $\mathcal{R} = 40a_0$. We match the inner-region solutions to solutions outside $\mathcal{R}$ that include channel coupling due to long-range induced dipole and quadrupole interactions and obtain, separately for each pair (J, π), K matrices, scattering phase shifts, and partial cross sections. All details of this calculation are described in our previous publication [1].

In this paper we use the fundamental dynamical data of the scattering calculation just outlined as given by the energy-dependent K matrices. For this purpose we have developed a computer code that reads the K matrices and combines them into scattering amplitudes. In the Appendix we analytically derive the scattering amplitude from the jj-coupled K matrices by using a sequence of spherical-wave decompositions and recoupling operations. Even though the spirit of this procedure has been outlined before (e.g., see [19, 20]), to the best of our knowledge it has not yet been published for the jj-coupling case of relevance here. In terms of the scattering amplitude f for the scattering of electrons with initial momentum $\mathbf{k}_0$, initial spin orientation m_0, final momentum $\mathbf{k}$, and final spin orientation m from targets in the initial state $\underline{\gamma}_0 = \underline{n}_0, \underline{\ell}_0, \underline{j}_0, \underline{m}_0^j$, and the final state $\underline{\gamma} = \underline{n}, \underline{\ell}, \underline{j}, \underline{m}^j$ ($\underline{n}$, $\underline{\ell}$, $\underline{j}$, and $\underline{m}^j$ are the usual quantum numbers that identify bound orbitals of the Dirac equation for an attractive central potential; in order to facilitate the distinction between valence and continuum orbitals, we underline quantum numbers that designate valence orbitals), the *spin-dependent* differential cross section is given by

$$\frac{d\sigma}{d\Omega}\left(\mathbf{k}\, m\, \underline{\gamma} \leftarrow \mathbf{k}_0\, m_0\, \underline{\gamma}_0\right) = \frac{k}{k_0}\left|f(\mathbf{k}\, m\, \underline{\gamma} \leftarrow \mathbf{k}_0\, m_0\, \underline{\gamma}_0)\right|^2 . \tag{1}$$

By averaging over the initial and by summing over the final spin orientations of projectile and target, the *spin-independent* differential cross section follows as

$$\frac{d\sigma}{d\Omega}\left(\mathbf{k}\, \tilde{\underline{\gamma}} \leftarrow \mathbf{k}_0\, \tilde{\underline{\gamma}}_0\right) = \frac{1}{2(2\underline{j}_0+1)} \sum_{\substack{m,m^j \\ m_0,m_0^j}} \frac{d\sigma}{d\Omega}\left(\mathbf{k}\, m\, \underline{\gamma} \leftarrow \mathbf{k}_0\, m_0\, \underline{\gamma}_0\right) , \tag{2}$$

with $\tilde{\underline{\gamma}}_0 = \underline{n}_0, \underline{\ell}_0, \underline{j}_0$ and $\tilde{\underline{\gamma}} = \underline{n}, \underline{\ell}, \underline{j}$.

For spin-independent electrons and spin-independent targets, the scattering system is rotationally invariant with respect to the direction $\mathbf{k}_0$ of the incident electrons. Total integrated and momentum-transfer cross sections are therefore given by

$$\sigma_{\rm tot}\left(\mathbf{k}\, \tilde{\underline{\gamma}} \leftarrow \mathbf{k}_0\, \tilde{\underline{\gamma}}_0\right) = 2\pi \int_0^\pi d\theta \sin\theta \frac{d\sigma}{d\Omega}\left(\mathbf{k}\, \tilde{\underline{\gamma}} \leftarrow \mathbf{k}_0\, \tilde{\underline{\gamma}}_0\right) \tag{3}$$

$$\sigma_{\rm mom}\left(\mathbf{k}\, \tilde{\underline{\gamma}} \leftarrow \mathbf{k}_0\, \tilde{\underline{\gamma}}_0\right) = 2\pi \int_0^\pi d\theta \sin\theta(1-\cos\theta) \times \frac{d\sigma}{d\Omega}\left(\mathbf{k}\, \tilde{\underline{\gamma}} \leftarrow \mathbf{k}_0\, \tilde{\underline{\gamma}}_0\right) ,$$

where θ denotes the scattering angle. In the limit of vanishing scattering energy ($k_0 \to 0$), the differential cross section becomes isotropic and $\sigma_{\rm mom} = \sigma_{\rm tot}$.

We used the Dirac R-matrix method to obtain K matrices for energies between 5×10^{-5} and 2.8 eV and for the 20 lowest scattering symmetries ($J = 0, \ldots, 9$ and both parities). We found that this number of scattering symmetries is sufficient to produce total cross sections (elastic and inelastic) [1], momentum-transfer cross sections, and inelastic differential cross sections that are converged for kinetic energies of the incident electrons not exceeding

2.8 eV. Within the same range of energies we observed that the elastic differential cross sections are almost, but not fully, converged. In order to obtain fully converged elastic differential cross sections, we also included scattering symmetries with $10 \leq J \leq 50$ (or partial waves up to $\ell = 51$), by using the effective range formula of O'Malley, Spruch, and Rosenberg [21] for the elastic K-matrix elements,

$$K_{ij} = \frac{\pi \alpha_d k_i^2}{(2\ell_i + 3)(2\ell_i + 1)(2\ell_i - 1)} \delta_{ij} , \quad (4)$$

where k_i and ℓ_i are the translational and orbital angular momentum of the scattered electron in channel i. We determined the *atomic* dipole polarizability α_d by solving (4) for α_d with K_{ii} taken from the highest partial waves included in our Dirac R-matrix calculation. For $J \leq 9$ or $\ell \leq 10$ we found convergence to $\alpha_d \approx 400 a_0^3$ as J or ℓ increases and used this value in (4) for all higher ($J \geq 10$) symmetries.

III. RESULTS AND DISCUSSION

This section contains our results for the angle-differential cross section $d\sigma/d\Omega$ (2) and the momentum-transfer cross section $\sigma_{\rm mom}$ (3). We consider an unpolarized monochromatic beam of incident electrons with kinetic energies between 5×10^{-5} and 2.8 eV and unpolarized cesium atoms in the $6s_{1/2}\,{}^2S_{1/2}$ ground state as targets.

A. Elastic angle-differential cross sections

Figure 1 shows the elastic differential cross section as a function of the energy E of the incident electrons and the scattering angle θ. Close to the elastic threshold [Fig. 1(a)] the cross sections are strongly enhanced by a triplet of $6s6p\,{}^3P_J^o$ resonances. These resonances have been discussed before as they appear in the total integrated cross section [1, 12]. They are normally ordered with the lowest term (in energy) corresponding to $J = 0$, the next higher term to $J = 1$, and the highest term to $J = 2$. The position E and width Γ of each term have been given in [12] as $E = 1.78$ eV, $\Gamma = 0.42$ eV ($J = 0$); $E = 5.56$ eV, $\Gamma = 2.43$ eV ($J = 1$); $E = 12.76$ eV, $\Gamma = 9.32$ eV ($J = 2$).

Regarded as a function of θ and for fixed E, the very-low-energy differential cross section shows a pronounced $\cos^2\theta$-like behavior due to dominant contributions from p-wave scattering. In the energy range below 20 meV forward and backward scattering are favored and about equally likely. For energies E around 100 meV, the p-wave character still dominates the differential cross section [Fig. 1(b)]. As E is further increased, however, p-wave scattering quickly loses influence due to the stronger admixture of higher partial waves. At energies E around 1 eV a local maximum appears at $\theta \approx 90°$ due to increasingly important d-wave scattering. At the same time the cross section becomes strongly forward peaked, and backward scattering only yields a relatively small contribution to the total integrated cross section.

The steplike structure at $E \approx 1.4$ eV is related to the two first inelastic thresholds which appear at 1.386 eV ($6s \rightarrow 6p_{1/2}$ excitation) and 1.455 eV ($6s \rightarrow 6p_{3/2}$ excitation). A multiplet of narrow $6p^2\,{}^3P_J^e$ resonances located at about 120 meV below the first inelastic threshold [1, 12] is not resolved in this figure. The widths of the $J = 0$, 1, and 2 terms of these resonances are 9 μeV, 150 μeV, and 1.33 meV, respectively, and are much smaller than the energy resolution of about 18 meV (corresponding to 150 equally spaced energy-mesh points) in Fig. 1(b).

In Fig. 2 we compare our results with the nonrelativistic two-state close-coupling calculation of Karule [5] for scattering energies of 0.1 to 0.6 eV. Despite striking differences in the conceptual and numerical treatment of the scattering problem, the two calculations agree fairly well in this region of low energies. At slightly higher energies, measured differential cross sections become available. Figure 3 shows the relative experimental cross section of Gehenn and Reichert [8], normalized to our results at $\theta \approx 90°$, together with the two calculations of Fig. 2. The agreement between the three sets of results is fairly good, except for the angular region around $\theta = 135°$ (corresponding to one of the local minima in d-wave dominated scattering) at $E = 0.8$, 1.0, and 1.2 eV. In this angular region the count rate is about two orders of magnitude smaller than in forward direction and the semilogarithmic plot overemphasizes the discrepancies between the results of Refs. [5] and [8] and our calculation. Neither the finite energy resolution of $\Delta E = 90$ meV, nor the angular resolution of $\Delta\theta = 8°$, nor the method of energy calibration in the experiment of Gehenn and Reichert appear suitable as an explanation for the mismatch at $\theta \approx 135°$ of our results and the experiment in Figs. 3(a)–3(c). At $E = 1.4$ eV [Fig. 3(d)] the agreement between both theories and experiment is exceptionally good, even in the angular region around $\theta = 135°$. This is also true for the comparison of experiment and theory at energies above the $6p_{3/2}$ excitation threshold [Figs. 4(a)–4(c)]. We notice that our elastic differential cross sections agree particularly well with the experiment for energies above the first [Fig. 3(d)] and higher [Fig. 4(a)–4(c)] inelastic thresholds.

In previous publications [1, 12] we compared total

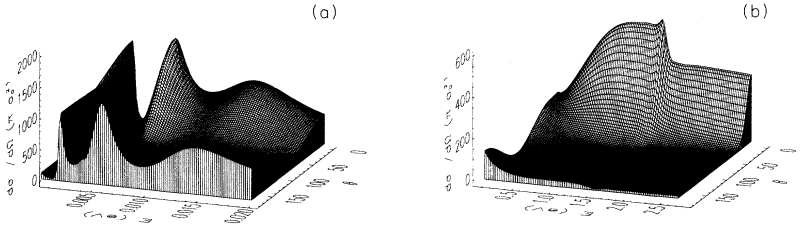

FIG. 1. Angle-differential cross section [in units of πa_0^2/sr ($\pi a_0^2 = 0.8798 \times 10^{-20}$ m^2)] for elastic scattering as a function of the incident electron's kinetic energy E (in eV) and the scattering angle θ (in degrees). (a) $E = 0$–20 meV; (b) $E = 0.1$–2.7 eV.

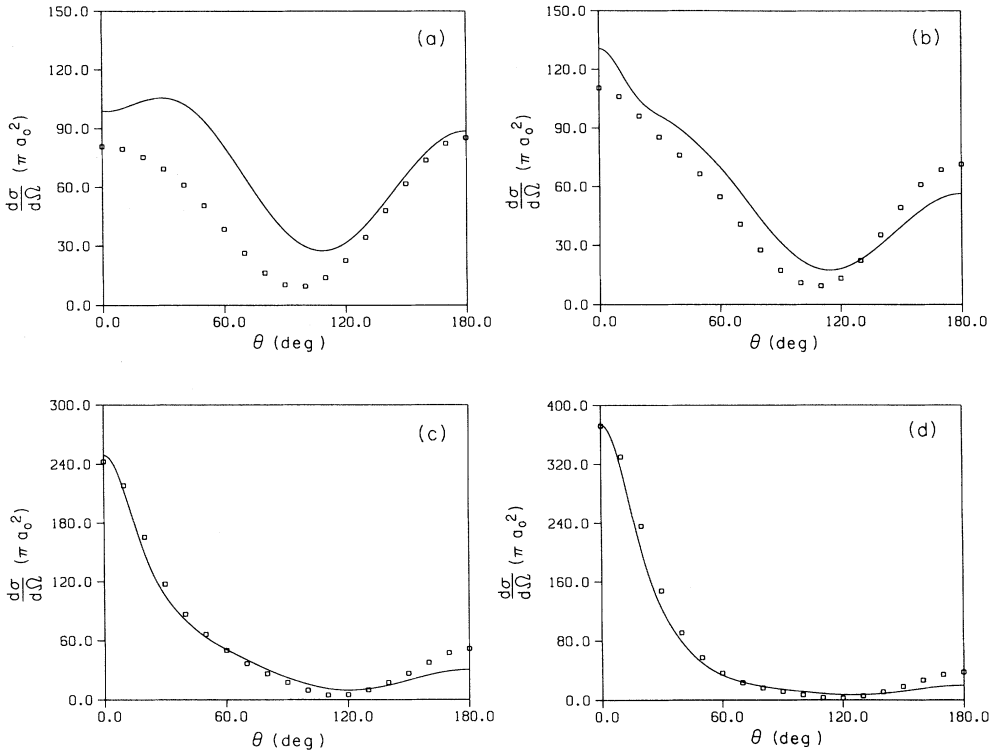

FIG. 2. Angle-differential cross section (in units of πa_0^2/sr) for elastic scattering as a function of the scattering angle θ (in degrees): ————, present Dirac R-matrix calculation; □, calculation of Karule [5]. (a) Electrons incident with $E = 0.1$ eV; (b) $E = 0.2$ eV; (c) $E = 0.4$ eV; (d) $E = 0.6$ eV.

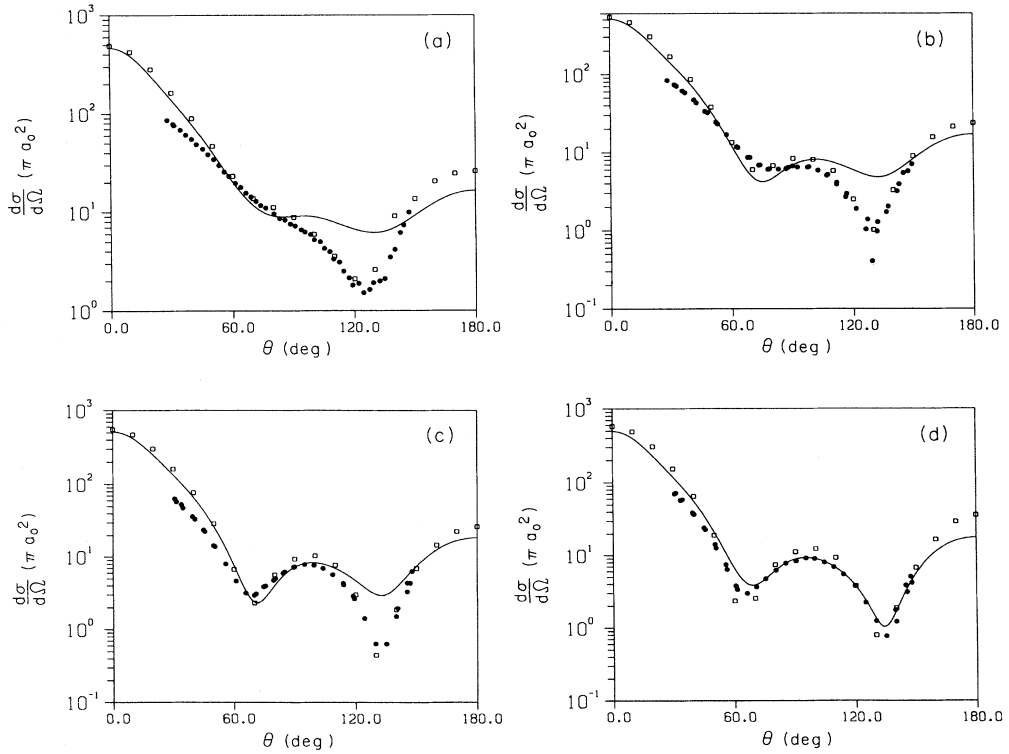

FIG. 3. As in Fig. 2. The relative experimental data of Gehenn and Reichert [8] (•) are normalized to our results at $\theta \approx 80°$ [Fig. 3(a)] and $\theta \approx 90°$ [Figs. 3(b)–3(d)]. (a) $E = 0.8$ eV; (b) $E = 1$ eV; (c) $E = 1.2$ eV; (d) $E = 1.4$ eV.

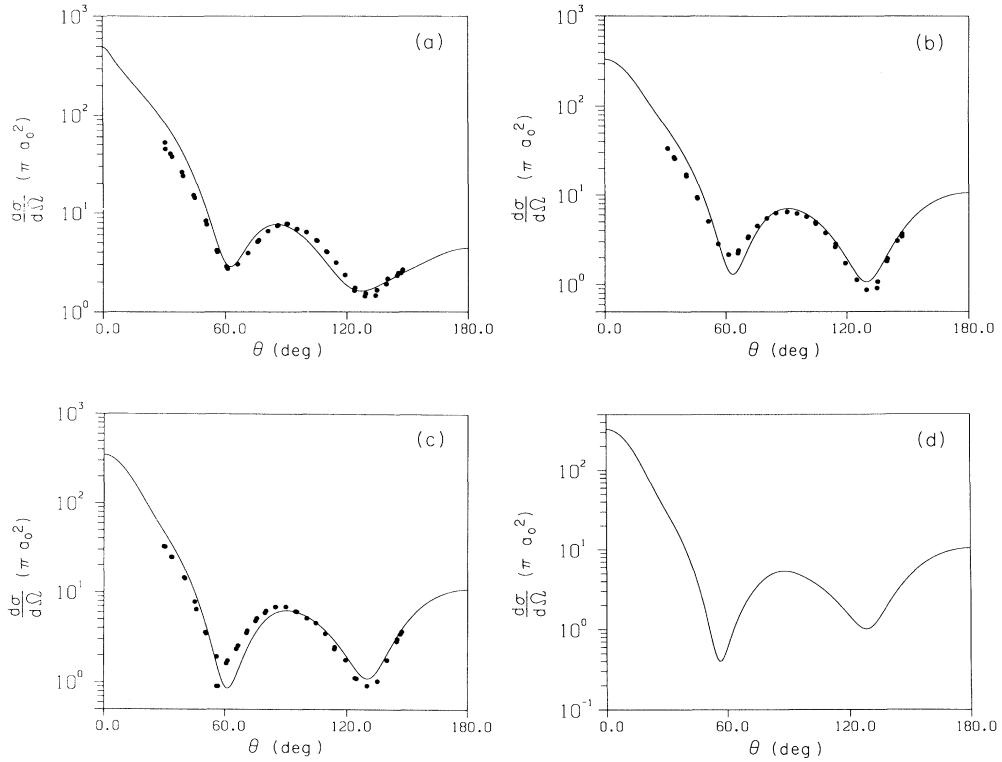

FIG. 4. As in Fig. 3. (a) $E = 1.6$ eV; (b) $E = 1.8$ eV; (c) $E = 2.0$ eV; (d) $E = 2.5$ eV, no experimental data available.

angle-integrated cross sections, derived from our Dirac R-matrix ansatz, with the theoretical results of Scott *et al.* [10]. The work of Scott *et al.* is based on the Schrödinger equation and takes relativistic one-particle interactions into account perturbatively. It differs further from our calculation in the precise choice of the core potentials. Otherwise, the two calculations are similar in spirit in that both include five close-coupled target states, a comparable number of continuum orbitals per channel, and relativistic effects. We found before [12] that our angle-integrated cross sections agree rather poorly with the results of Scott *et al.* [10]. It is therefore not surprising that the angle-differential cross sections only agree within an order of magnitude (Fig. 5), even though they display similar features at different scattering energies.

Our differential cross sections in Fig. 5 display structures at scattering energies close to the $6p_j$ inelastic thresholds [compare also Fig. 1(b)]. Gehenn and Reichert [8] interpreted structure seen in their measured elastic differential cross section at $E = 1.49 \pm 0.02$ eV as the $^3F^o$ resonance predicted earlier [3, 6] at 1.6–1.7 eV. We find excellent agreement with the shape of their measured cross section at 1.49 eV, while confirming our earlier prediction [1] that the $^3F^o$ resonance lies at a higher energy (1.62 eV, J averaged). Moreover, we do not find evidence for $^3F^o$ resonances in the elastic cross section, in accord with our previous [1] finding that this resonance is predominantly formed by $6p_j 5d_{j'}$ configurations and thus appears preferentially in inelastic channels.

B. Inelastic angle-differential cross sections

The inelastic differential cross sections for $6s \rightarrow 6p_{1/2}$ [Fig. 6(a)] and $6s \rightarrow 6p_{3/2}$ excitation [Fig. 6(b)] display a striking structure near the inelastic thresholds. This structure is due to the above-mentioned $^3F^o$ resonance at the J-averaged energy $E = 1.62$ eV. As in the case of elastic scattering, the inelastic cross sections become strongly forward peaked as the scattering energy exceeds the close-to-threshold region. We emphasize that without relativistic interactions, the plots in Figs. 6(a) and 6(b) would look alike, and the corresponding inelastic cross sections would differ by a statistical branching ratio of exactly two (there are twice as many magnetic sublevels in the $6p_{3/2}$ state as there are in the $6p_{1/2}$ state). Note that the statistical branching ratio is "factored out" in the two subplots in Fig. 6; the two z axes differ by a factor of 2. Comparison of the two subplots in Fig. 6 elucidates relativistic interactions through (i) fine-structure split excitation thresholds and (ii) deviation from the statistical branching ratio, which is particularly striking for forward scattering at the highest shown energies, as well as for the angular distributions at energies close to thresholds and structures associated with the $^3F^o$ resonance.

In Fig. 7 we show the inelastic differential cross sections for $6s \rightarrow 6p_j$ excitation for two energies ($E = 1.632$ and 2.04 eV) in comparison with the results of Scott *et al.* [10]. As mentioned before, the two calculations show significant differences in the total angle-integrated cross sec-

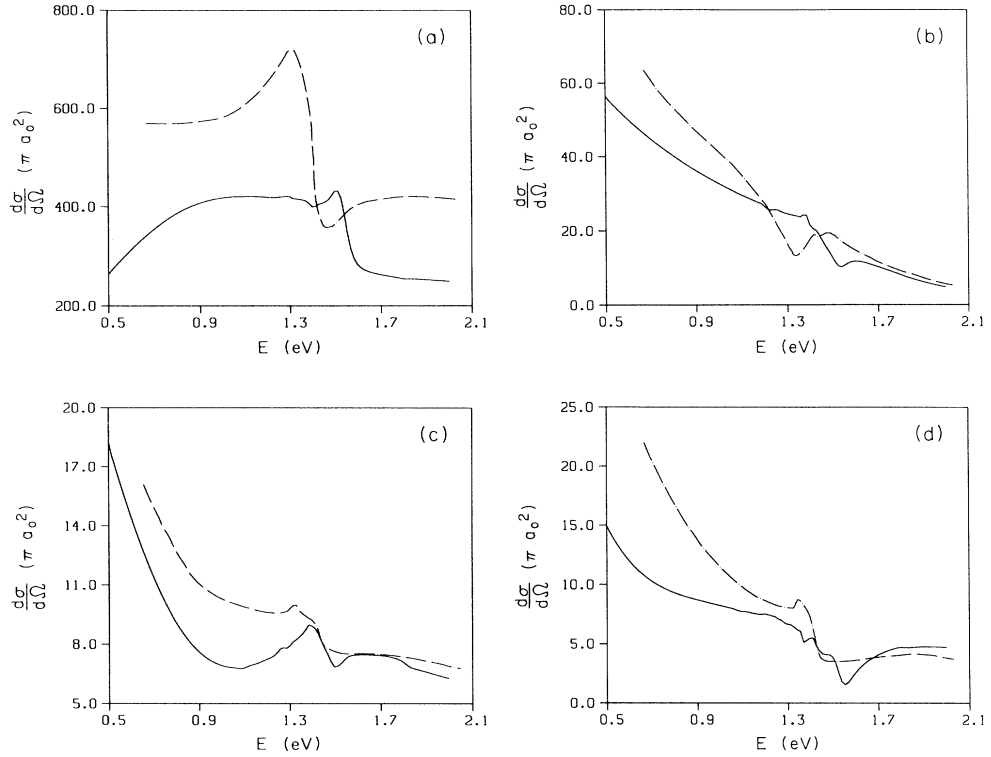

FIG. 5. Angle-differential cross sections (in units of πa_0^2/sr) for elastic scattering as a function of the incident electron's energy: ————, present Dirac R-matrix calculation; — · — · — ·, calculation of Scott *et al.* [9]. (a) Scattering angle $\theta = 10°$; (b) $\theta = 50°$; (c) $\theta = 90°$; (d) $\theta = 150°$.

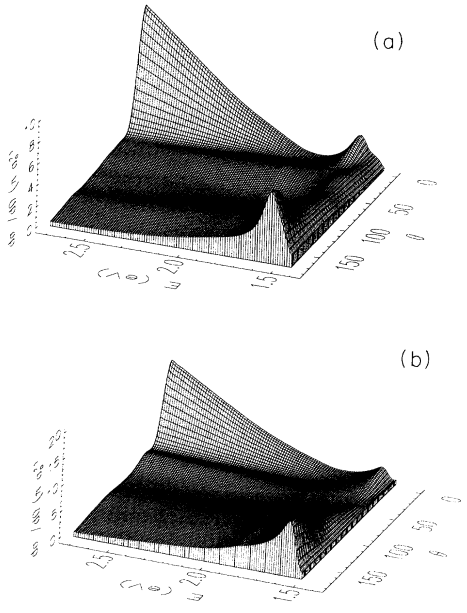

FIG. 6. Angle-differential cross section (in units of πa_0^2/sr) for inelastic scattering for electrons incident with less than 2.7-eV kinetic energy. (a) $6s \rightarrow 6p_{1/2}$ excitation; (b) $6s \rightarrow 6p_{3/2}$ excitation. The perpendicular axis differ by a factor of 2 such that for a purely statistical branching ratio and no fine-structure splitting (a) and (b) would look identical.

tions [12] and also for the angle-differential cross sections. Nevertheless, they agree within an order of magnitude, and, at $E = 2.04$ eV, share some qualitative features. Again the nonstatistical branching ratio for excitation of the two fine-structure split cesium levels can be very easily seen by comparing Figs. 7(a) with 7(b), and 7(c) with 7(d).

C. Momentum-transfer cross sections

We derive angle-integrated cross sections σ_{tot} and momentum-transfer cross sections σ_{mom} for spin-independent elastic scattering by numerical integration of the angle-differential elastic cross section $d\sigma/d\Omega$ according to Eq. (3). As a test, we also calculated σ_{tot} directly from the K matrices (for details see Ref. [1]), i.e., without referring to the recoupling operation described in the Appendix. Agreement of the two calculations of σ_{tot} gives evidence for the correct analysis and programming of the recoupling operations necessary to express $d\sigma/d\Omega$ in terms of K matrices. It proves that the lowest moment of $d\sigma/d\Omega$ with respect to an expansion in Legendre polynomials of $\cos\theta$ is reproduced correctly by the recoupling calculation.

Our results for σ_{mom} in comparison with σ_{tot} are shown in Fig. 8. Figure 8(a) contains the cross sections for scattering energies E from extremely close to the elastic threshold up to $E = 0.1$ eV. To the best of our knowl-

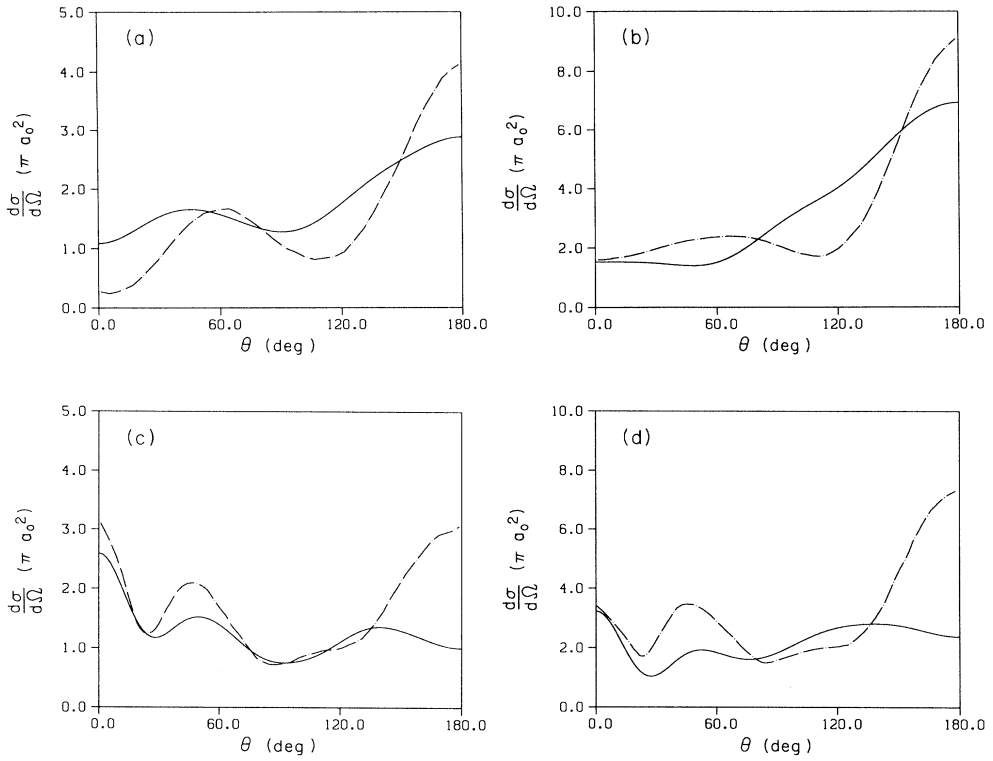

FIG. 7. Angle-differential cross sections (in units of πa_0^2/sr) for inelastic scattering for excitation of both $6p_j$ fine-structure levels of cesium as a function of the scattering angle θ (in degrees): ————, Dirac R-matrix calculation; — · — · — ·, calculation of Scott *et al.* [10]. (a) $6s \rightarrow 6p_{1/2}$ excitation, $E = 1.632$ eV; (b) $6s \rightarrow 6p_{3/2}$ excitation, $E = 1.632$ eV; (c) $6s \rightarrow 6p_{1/2}$ excitation, $E = 2.04$ eV; (d) $6s \rightarrow 6p_{3/2}$ excitation, $E = 2.04$ eV.

edge this is the first direct calculation of σ_{mom} and σ_{tot} in this very-low-energy region. Since scattering is ultimately isotropic as $E \rightarrow 0$, σ_{mom} and σ_{tot} become identical for the lowest energies shown. The dominant feature in Fig. 8(a) is the multiplet of $6s6p\,^3P_J^o$ resonances, which are normally ordered with the $J = 0$ component corresponding to the peak with the lowest energy and the $J = 2$ component corresponding to the peak with the highest energy [1, 12]. The same cross sections as in Fig. 8(a) are shown in Fig. 8(b) for 0.1 eV $\leq E \leq$ 2.8 eV. For these energies the elastic differential cross section is forward peaked [cf. Fig. 1(b)] such that $\sigma_{\text{mom}} < \sigma_{\text{tot}}$. Structures related to a multiplet of $^3P_J^e$ resonances [1, 12] below the $6p_{1/2}$ threshold and the detailed behavior of the cross sections at the $6p_j$ thresholds are not resolved. Nevertheless, the opening of inelastic channels is clearly visible as the steplike structure in σ_{mom} and σ_{tot} at $E \approx 1.4$ eV.

In Fig. 9 we compare our results for σ_{mom} in the energy range of Fig. 8(a) and 8(b) with data from the literature [2, 13–16]. Fabrikant [13] used effective-range theory to extrapolate (below $E = 0.1$ eV) theoretical phase shifts calculated (for $E \geq 0.1$ eV) by Karule [3]. Since the uncorrected extrapolation of Karule's data leads to the prediction of a bound $^3P^o$ state of Cs^- and to disagreement with experimental data, Fabrikant readjusted the polarizability of cesium as well as effective-range parameters using experimental data for the broadening and shift of cesium Rydberg levels perturbed by cesium atoms. Above about 15 meV his momentum-transfer cross section is monotonically decreasing in E, in qualitative agreement with our result. Also in agreement with our calculation, Fabrikant's cross section shows no evidence for the striking structures displayed in the remaining curves in Fig. 9. The physical origin of the maximum at $E \approx 15$ meV in Fabrikant's work is subject to some speculation due to uncertainties in his adjusted effective-range extrapolation. If this maximum is not an artifact of the extrapolation method, the agreement of its position with the $J = 2$ term of the $^3P^o$ resonance in our calculation suggests that it also originates in this resonance (either in the $J = 2$ term or including all $^3P_J^o$ terms), in accordance with Fabrikant's assumption of a $^3P^o$ resonance.

Fabrikant identifies the minimum at $E \approx 5$ meV in his curve as a Ramsauer-Townsend minimum, whereas we obtained the Ramsauer-Townsend minimum at ≈ 50 meV [1]. Again excluding artifacts of his extrapolation method, the comparison of Fabrikant's and our curve suggests that the minimum Fabrikant obtained is related to the onset of the resonances at $E \approx 1$ meV in our curve (the exact position of which is hidden by the multiplet of $^3P^o$ resonances).

Stefanov [15], Nighan and Postma [14], and Postma [16] derived momentum-transfer cross sections by fitting transport coefficients obtained from various experiments, such as electron-cyclotron resonance measurements and

measurements of electrical and thermal conductivities of electrons in cesium vapors. The extraction of cross sections from these experimental data is very difficult and, in principle, amounts to inverting a transport equation (the Boltzmann equation for the transport of electrons in cesium vapor) and unfolding the product of the electron-velocity distribution and the cross section. Stefanov's result for $\sigma_{\rm mom}$ shows a pronounced minimum at $E \approx 0.26$ eV in clear contrast to the work of Fabrikant [13] and to our calcualtion (Fig. 9). With respect to total cross sections measured by Visconti, Slevin, and Rubin [4] which, in the same energy interval, decrease monotonically in E, Visconti speculates that the monotonic behavior of $\sigma_{\rm tot}$ is not necessarily incompatible with oscillating structures in $\sigma_{\rm mom}$ due to either the higher sensitivity of $\sigma_{\rm mom}$ to large-angle scattering or due to the relatively large energy spread of the electron beam in his experiment. In agreement with Fabrikant's results, however, our calculation suggests that this is not true. Furthermore, the total cross sections of Visconti *et al.* are six to 20 times larger

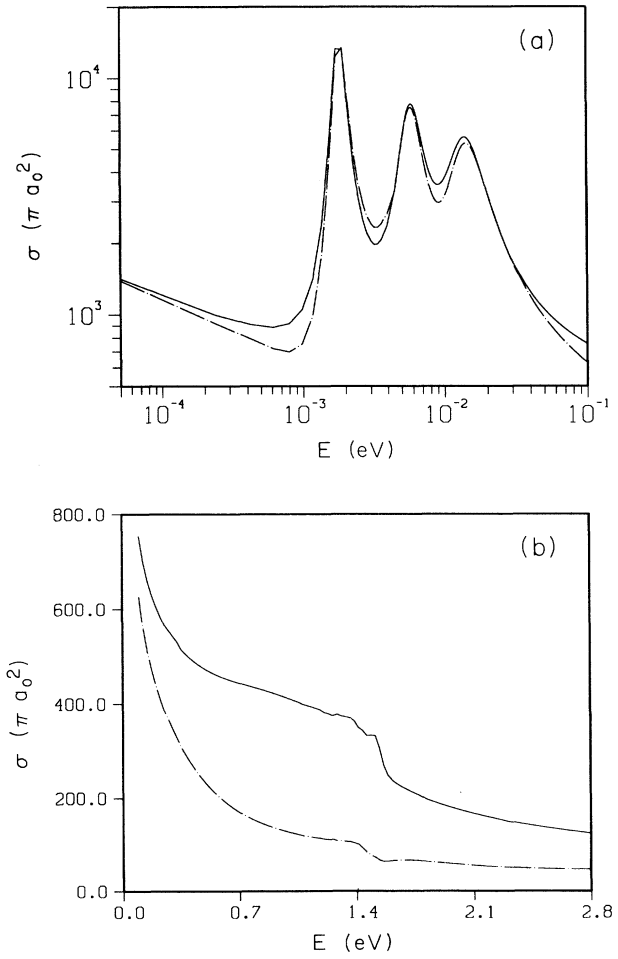

FIG. 8. Total integrated cross section (————) and momentum-transfer cross section (— · — · — ·) (in units of πa_0^2) from the present Dirac R-matrix calculation. (a) $E = 5 \times 10^{-5}$ eV–0.1 eV; (b) 0.1–2.8 eV, elastic contribution only.

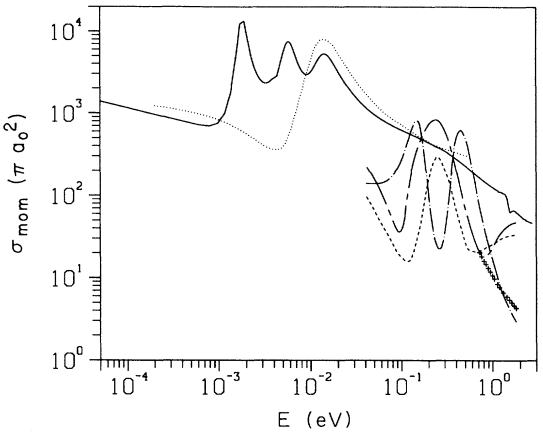

FIG. 9. Momentum-transfer cross section (in units of πa_0^2) for elastic scattering: ————, Dirac R-matrix calculation; · · · · · ·, Fabrikant [13]; — · — · — ·, Stefanov [15]; — – — – —, Nighan and Postma (taken from [15]); – – – – –, Crown and Russek (taken from [15]); ++++++ Postma (taken from [15]).

than the momentum-transfer cross sections of Stefanov, whereas the comparison of $\sigma_{\rm mom}$ and $\sigma_{\rm tot}$ in our calculation for energies between 100 meV and 1 eV [cf. Fig. 8(b)] indicates that $\sigma_{\rm tot}$ exceeds $\sigma_{\rm mom}$ by not more than a factor of about 4. It is interesting to note that the results of Nighan and Postma [14] contradict those of Stefanov [15] in the sense that Nighan and Postma predict a maximum for $\sigma_{\rm mom}$ where Stefanov's cross section has a local minimum (Fig. 9). Here it is worth mentioning that the method used by Nighan and Postma to extract $\sigma_{\rm mom}$ from electron drift-velocity data is not unique and does not permit one to locate maxima or minima precisely [15]. Nighan and Postma therefore chose the maximum of $\sigma_{\rm mom}$ in accordance with the calculation of Crown and Russek [2] which is based on a perturbatively determined potential for the electron-cesium interaction and not expected to guarantee accurate results for the considered low-scattering energies.

D. Total integrated cross sections

Very recently, Jaduszliwer and Chan [11] reported the measurement of total integrated cross sections for electron-cesium scattering between $E = 2$ and 18 eV. In Fig. 10 we show our previously published [1, 12] compilation of calculated and measured total integrated cross sections supplemented by the new experimental values [11] at 2 and 3 eV.

IV. SUMMARY AND CONCLUSIONS

In this work we used the fundamental dynamical data of a previously described Dirac R-matrix calculation [1, 12] in order to derive elastic and inelastic angle-differential cross sections for the scattering of slow unpolarized electrons off neutral unpolarized cesium atoms. Starting from energy-dependent K matrices that include

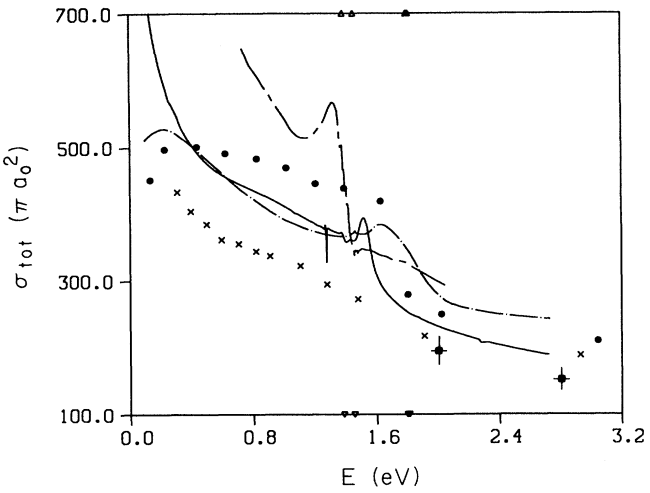

FIG. 10. Total integrated cross section (in units of πa_0^2 and including elastic and inelastic contributions) for low-energy e^--Cs scattering. Theory: present Dirac R-matrix calculation (Ref. [1]) (————); Ref. [6] (— · — · — ·); Ref. [9] (— - — -); Ref. [3] (•). Experiment: Ref. [4] (×); Ref. [11] (■). The $6p_{1/2,3/2}$ and $5d_{3/2,5/2}$ thresholds are marked by the small triangles.

all the dynamical information of the electron-cesium scattering system, we used standard recoupling and partial-wave expansion methods to analytically derive the spin-dependent (with respect to both target and projectile) scattering amplitude. The scattering amplitude makes a variety of observables easily accessible. In a first attempt to use the Dirac R-matrix method to obtain *angle-dependent* scattering information we utilized these scattering amplitudes to derive spin-independent angle-differential and momentum-transfer cross sections. We compared our angle-differential cross sections with experimental and theoretical data from the literature and found in most cases, and in particular for the only available elastic experimental data of Gehenn and Reichert [8], fair or good agreement. With respect to inelastic scattering, the angle-differential cross sections for $6s \rightarrow 6p_{1/2}$ and $6s \rightarrow 6p_{3/2}$ excitation deviate from a purely statistical branching ratio and therefore indicate the importance of relativistic effects which are properly taken into account in our relativistic treatment of the scattering process. The inelastic cross sections show an interesting structure which we related to a $6p5d\,^3F^o$ resonance mentioned before by Karule [3], Burke and Mitchell [6], and Gehenn and Reichert [8].

After numerical integration of the angle-differential cross section, we obtained total and momentum-transfer cross sections ($\sigma_{\rm tot}$ and $\sigma_{\rm mom}$). The total cross sections obtained by this angle integration agree with the result we previously [1, 12] derived in a different way (directly from the K matrices and without using the sequence of recoupling transformations and partial-wave expansions outlined in the Appendix), thus providing additional evidence that the analytical derivation of the scattering amplitude (cf. the Appendix) and its numerical implementation are correct. Our results for $\sigma_{\rm mom}$ cover the energy range (0.1–1 eV) of primary interest for plasma applications such as, e.g., for the development of thermionic converters [17], and, for the first time include the immediate vicinity of the elastic threshold. The direct calculation within a close-coupling approach of $\sigma_{\rm mom}$ at these low energies is expected to be of higher accuracy and more reliable than indirect methods [13–16] that refer to the measurement of thermal and electrical conductivities in swarm experiments [14–16] and to the collisional broadening of cesium Rydberg levels [13]. Due to the rather indirect and complicated extraction of $\sigma_{\rm mom}$ from transport coefficients obtained from electron-cesium swarm experiments [14–16], it is not surprising that the extracted $\sigma_{\rm mom}$ are contradictory and disagree with our results. Of particular interest in our results is the strong enhancement of $\sigma_{\rm mom}$ at very low energies due to a multiplet of $^3P_J^o$ resonances, which we identified before in $\sigma_{\rm tot}$ [1, 12] and for which evidence exists in the extrapolated semiempirical momentum-transfer cross sections of Fabrikant [13].

The results presented in this paper rely on our Dirac R-matrix code [1] and on a new program that converts K matrices into spin-dependent scattering amplitudes. We plan to use these amplitudes to derive other observables, such as electron spin-polarization parameters (generalized STU parameters [22]) and Stokes parameters that describe the characteristics of light emitted from collisionally excited cesium atoms [23]. We further intend to perform similar calculations for other alkali-metal-like targets.

ACKNOWLEDGMENTS

It is our pleasure to thank Michael A. Morrision for discussions on the content of the appendix to this work and on the interpretation of swarm measurements. One of us (U.T.) acknowledges financial assistance by Rasor Associates, Inc., in Sunnyvale, CA. This work was supported by the U. S. Department of Energy, Office of Fusion Energy.

APPENDIX: DERIVATION OF THE SCATTERING AMPLITUDE FROM jj-COUPLED K MATRICES

In this appendix we derive the spin-dependent amplitude for electron scattering from alkali-metal-like (i.e., basically one-electron) targets. We start from jj-coupled K (or reactance) matrices as they may be provided by a Dirac R-matrix calculation (for details see Ref. [1]). The K matrices contain all the dynamical information of the scattering process and are related to the scattering matrices S and the T matrices by

$$\mathbf{S} = \frac{1 + i\mathbf{K}}{1 - i\mathbf{K}} \quad \text{and} \quad T_{\nu'\nu} = S_{\nu'\nu} - \delta_{\nu'\nu} \,. \tag{A1}$$

The elements of the K, S, and T matrices are defined with respect to scattering channels ν. In a relativistic (i.e., jj-coupled) scattering calculation, in which only two electrons are explicitly taken into account, each chan-

nel is specified by the set of quantum numbers

$$\nu = \underline{n}\ \underline{\ell}\ \underline{j}\ \ell\ j\ J\ \pi\ , \tag{A2}$$

where the underlined quantities are the principal quantum number, the orbital angular momentum $\underline{\ell}$, and the total angular momentum $\underline{j}$ of the target. The scattered electron has the orbital angular momentum ℓ and the total angular momentum j. The total angular momentum and parity of the scattering system (containing the two electrons) are denoted by the good quantum numbers J and π.

The set of quantum numbers (A2) is chosen partly for computational convenience. For electron scattering, J and π are not directly observable and measurements usually yield quantities such as cross sections, which include *sums* over J and π. Nevertheless the computational advantage of keeping track of J and π is striking, since the total Hamiltonian is block diagonal in these quantum numbers. Similarly, the computational advantage of relating channels to ℓ and j is evident, whereas these quantities are not directly accessible in defining asymptotic scattering states of immediate physical relevance.

On the other hand, the scattering amplitude f is defined with respect to asymptotic scattering states given by the scattered electron's momentum $\mathbf{k}_0$ (a long time) before and $\mathbf{k}$ (a long time) after the interaction with the target, its spins m_0, and m before and after the interaction, and the initial and final states of the target $\underline{\gamma}_0$ and $\underline{\gamma}$, given by

$$\begin{aligned} \underline{\gamma}_0 &= \tilde{\underline{\gamma}}_0\ \underline{m}_0^j\ = \underline{n}_0\ \underline{\ell}_0\ \underline{j}_0\ \underline{m}_0^j \\ \underline{\gamma} &= \tilde{\underline{\gamma}}\ \underline{m}^j\ = \underline{n}\ \underline{\ell}\ \underline{j}\ \underline{m}^j\ . \end{aligned} \tag{A3}$$

The magnetic quantum numbers $\underline{m}_0^j$ and $\underline{m}^j$ are the projections of $\underline{j}_0$ and $\underline{j}$ onto the (not yet specified) quantization axis. The sets of quantum numbers $\tilde{\underline{\gamma}}_0$ and $\tilde{\underline{\gamma}}$ denote the initial and final state of the target irrespective of its spin orientation, i.e., $\tilde{\underline{\gamma}}_0 = \underline{n}_0\ \underline{\ell}_0\ \underline{j}_0$ and $\tilde{\underline{\gamma}} = \underline{n}\ \underline{\ell}\ \underline{j}$. With respect to the abstract operator equivalent $\hat{T}$ to the T matrix defined in (A1), the scattering amplitude is defined by

$$f(\mathbf{k}\ m\ \underline{\gamma} \leftarrow \mathbf{k}_0\ m_0\ \underline{\gamma}_0\ ) = 2\pi i \left\langle \mathbf{k}\ m\ \underline{\gamma} \mid \hat{T} \mid \mathbf{k}_0\ m_0\ \underline{\gamma}_0 \right\rangle\ . \tag{A4}$$

In order to relate the matrix elements of $\hat{T}$ in the "physical basis" $|\mathbf{k}\ m\ \underline{\gamma}\rangle$ to the known T-matrix elements, $T_{\nu\nu'} = \langle\nu|\hat{T}|\nu'\rangle$, we have to perform a spherical-wave decomposition and a series of recoupling transformations. The representation of $\hat{T}$ in (A4) is called the *uncoupled plane-wave representation.* In what follows we adopt the phase convention of Condon and Shortley [24].

(1) *Spherical wave decomposition.* We decompose the plane-wave states $|\mathbf{k}_0\rangle$ and $|\mathbf{k}\rangle$ of the scattered electron according to

$$|\mathbf{k}\rangle = \int dE \sum_{\ell,m^\ell} |E\ \ell\ m^\ell\rangle\langle E\ \ell\ m^\ell|\mathbf{k}\rangle,$$

$$\langle E\ \ell\ m^\ell|\mathbf{k}\rangle = i^\ell\ k^{-1/2}\ \delta(E - E_k)\ Y_\ell^{m^{\ell *}}(\mathbf{k})\ ,$$

with the magnetic quantum number m^ℓ corresponding to ℓ, and with

$$\langle\mathbf{r}|\mathbf{k}\rangle = (2\pi)^{-3/2}\ e^{i\mathbf{k}\cdot\mathbf{r}} \quad \text{and} \quad E_k = \tfrac{1}{2}k^2\ .$$

Formally introducing the unit operator

$$\mathbf{1} = \int dE \sum_{\ell,m^\ell} |E\ \ell\ m^\ell\rangle\langle E\ \ell\ m^\ell|$$

to the right and left of $\hat{T}$ in (A4), we find the amplitude in *uncoupled spherical representation*

$$f(\mathbf{k}\ m\ \underline{\gamma} \leftarrow \mathbf{k}_0\ m_0\ \underline{\gamma}_0) = 2\pi i\ (k_0 k)^{-1/2} \sum_{\ell,m^\ell} \sum_{\ell',m^{\ell'}} i^{\ell'-\ell}\ Y_\ell^{m^\ell}(\hat{\mathbf{k}})\ \langle E_k\ \ell\ m^\ell\ m\ \underline{\gamma} \mid \hat{T} \mid E_0\ \ell'\ m^{\ell'}\ m_0\ \underline{\gamma}_0\rangle\ Y_{\ell'}^{m^{\ell'*}}(\hat{\mathbf{k}}_0)\ , \tag{A5}$$

where $E_0 = \frac{1}{2}k_0^2$.

(2) *Coupling of the scattered electron's angular momentum* $\boldsymbol{l}$ *and spin* $\mathbf{s}$ *to* $\mathbf{j}$. The quantum numbers in the matrix element in (A5) may be regrouped such that

$$\langle E_k\ \ell\ m^\ell\ m\ \underline{\gamma} \mid \hat{T} \mid E_0\ \ell'\ m^{\ell'}\ m_0\ \underline{\gamma}_0\rangle = \langle \ell\ m^\ell\ \tfrac{1}{2}\ m|\langle E_k\ \ell\ \underline{\gamma} \mid \hat{T} \mid E_0\ \ell'\ \underline{\gamma}_0\rangle|\ell'\ m^{\ell'}\ \tfrac{1}{2}\ m_0\rangle\ .$$

Introducing the unit operator

$$\mathbf{1} = \sum_{j,m^j} |\ell\ \tfrac{1}{2}\ j\ m^j\rangle\langle \ell\ \tfrac{1}{2}\ j\ m^j|$$

twice, to the right of $\langle \ell\ m^\ell\ \frac{1}{2}\ m|$ and to the left of $|\ell'\ m^{\ell'}\ \frac{1}{2}\ m_0\rangle$, we see that the amplitude in *ls-coupled representation* reads

$$\begin{aligned} f(\mathbf{k}\ m\ \underline{\gamma} \leftarrow \mathbf{k}_0\ m_0\ \underline{\gamma}_0) = 2\pi i\ (k_0 k)^{-1/2} \sum_{j,j'} \sum_{\ell,m^\ell} \sum_{\ell',m^{\ell'}} & i^{\ell-\ell'}\ Y_\ell^{m^\ell}(\hat{\mathbf{k}})\ \langle \ell\ m^\ell\ \tfrac{1}{2}\ m|j\ m^j\rangle\langle E_k\ \ell\ j\ m^j\ \underline{\gamma} \mid \hat{T} \mid E_0\ \ell'\ j'\ m^{j'}\ \underline{\gamma}_0\rangle \\ & \times\langle j'\ m^{j'}|\ell'\ m^{\ell'}\ \tfrac{1}{2}\ m_0\rangle\ Y_{\ell'}^{m^{\ell'*}}(\hat{\mathbf{k}}_0)\ , \end{aligned} \tag{A6}$$

with the Clebsch-Gordan coefficients $\langle \ell\, m^\ell\, \frac{1}{2}\, m | j\, m^j \rangle$, and the magnetic quantum numbers corresponding to j and j',

$$m^j = m^\ell + m \quad , \quad m^{j'} = m^{\ell'} + m_0 \, . \tag{A7}$$

(3) *Coupling of* $\underline{\mathbf{j}}$ *and* $\mathbf{j}$ *to* $\mathbf{J}$. We first regroup the quantum numbers in the matrix element in (A6) such that

$$\langle E_k\, \ell\, j\, m^j\, \underline{\gamma} | \hat{T} | E_0\, \ell'\, j'\, m^{j'}\, \underline{\gamma}_0 \rangle = \langle j\, m^j\, \underline{j}\, \underline{m}^j | \langle E_k\, \ell\, j\, \tilde{\underline{\gamma}} | \hat{T} | E_0\, \ell'\, j'\, \tilde{\underline{\gamma}}_0 \rangle | j'\, m^{j'}\, \underline{j}_0\, \underline{m}_0^j \rangle \, .$$

Inserting the unit operator

$$\mathbf{1} = \sum_{J,M} | \underline{j}\, j\, JM \rangle \langle \underline{j}\, j\, JM |$$

twice, to the right of $\langle j\, m^j\, \underline{j}\, \underline{m}^j |$ and to the left of $| j'\, m^{j'}\, \underline{j}_0\, \underline{m}_0^j \rangle$, we obtain the amplitude in *jj-coupled representation*

$$\begin{aligned} f(\mathbf{k}\, m\, \underline{\gamma} \leftarrow \mathbf{k}_0\, m_0\, \underline{\gamma}_0) = 2\pi i\, (k_0 k)^{-1/2} \sum_J \sum_{j,j'} \sum_{\ell, m^\ell} \sum_{\ell'} & i^{\ell' - \ell} Y_\ell^{m^\ell}(\hat{\mathbf{k}})\, \langle \ell\, m^\ell\, \tfrac{1}{2} m | j\, m^j \rangle \langle j\, m^j\, \underline{j}\, \underline{m}^j | J\, M \rangle \\ & \times \langle E_k\, \ell\, j\, \tilde{\underline{\gamma}} | \hat{T} | E_0\, \ell'\, j'\, \tilde{\underline{\gamma}}_0 \rangle^J \\ & \times \langle J\, M | j'\, m^{j'}\, \underline{j}_0\, \underline{m}_0^j \rangle \langle j'\, m^{j'} | \ell'\, m^{\ell'}\, \tfrac{1}{2} m_0 \rangle\, Y_{\ell'}^{m^{\ell'} *}(\hat{\mathbf{k}}_0) \, , \end{aligned} \tag{A8}$$

where we have used the facts that the scattering process is independent of the orientation of the coordinate system [i.e., the matrix element of $\hat{T}$ in (A8) does not depend on M] and that J and M are good quantum numbers in writing

$$\langle E_k\, \ell\, j\, \tilde{\underline{\gamma}}\, J\, M | \hat{T} | E_0\, \ell'\, j'\, \tilde{\underline{\gamma}}_0\, J'\, M' \rangle = \delta_{JJ'}\, \delta_{MM'} \langle E_k\, \ell\, j\, \tilde{\underline{\gamma}} | \hat{T} | E_0\, \ell'\, j'\, \tilde{\underline{\gamma}}_0 \rangle^J \, .$$

Furthermore, the Clebsch-Gordan coefficients imply

$$M = m^{j'} + \underline{m}_0^j \quad \text{and} \quad m^{\ell'} = m^\ell + m - m_0 + \underline{m}^j - \underline{m}_0^j \, . \tag{A9}$$

Since the parity of the scattering system is conserved, it is convenient to explicitly separate the contributions from both parities in (A8). For this purpose we introduce the function

$$\Pi(\ell_1, \ell_2) = (-1)^{\ell_1 + \ell_2} \, ,$$

such that the initial- and final-state parities in (A8) are given by $\Pi(\ell', \ell_0)$ and $\Pi(\ell, \underline{\ell})$. Due to energy conservation, we do not need to keep track of E_k, which is given by

$$E_k = E_0 - \Delta\epsilon(\tilde{\underline{\gamma}} \leftarrow \tilde{\underline{\gamma}}_0) \, ,$$

where $\Delta\epsilon$ is the atomic excitation energy. Therefore the matrix element in (A8) may be considered as a function of E_0 and separately for each parity π. As the notation

$$\begin{aligned} T_{\nu'\nu} &= T^{J\pi}_{\tilde{\underline{\gamma}}\, \ell\, j,\, \tilde{\underline{\gamma}}_o\, \ell'\, j'}(E_0) \\ &= \langle E_k\, \ell\, j\, \tilde{\underline{\gamma}} | \hat{T} | E_0\, \ell'\, j'\, \tilde{\underline{\gamma}}_0 \rangle^{J\pi} \end{aligned} \tag{A10}$$

emphasizes we have completed the sequence of recoupling tranformations. The T-matrix elements in (A10) and (A11) are now identical and compatible with the channel designation and basic dynamical results of a relativistic close-coupling calculation as, i.e., the aforementioned Dirac R-matrix calculation [1]. The jj-coupled amplitude can now be rewritten as

$$\begin{aligned} f(\mathbf{k}\, m\, \underline{\gamma} \leftarrow \mathbf{k}_0\, m\, \underline{\gamma}_0) = 2\pi i\, (k_0 k)^{-1/2} \sum_{J,\pi} \sum_{j,j'} \sum_{\ell} \sum_{\ell'} & i^{\ell - \ell'}\, \delta_{\pi, \Pi(\ell, \underline{\ell})}\, \delta_{\pi, \Pi(\ell', \underline{\ell}_0)} \\ & \times \sum_{m^\ell} Y_\ell^{m^\ell}(\hat{\mathbf{k}}) \langle \ell\, m^\ell\, \tfrac{1}{2}\, m | j\, m^j \rangle \langle j\, m^j\, \underline{j}\, \underline{m}^j | JM \rangle\, T_{\nu'\nu} \\ & \times \langle J\, M | j'\, m^{j'}\, \underline{j}_0\, \underline{m}_0^j \rangle \langle j'\, m^{j'} | \ell'\, m^{\ell'}\, \tfrac{1}{2}\, m_0 \rangle\, Y_{\ell'}^{m^{\ell'} *}(\hat{\mathbf{k}}_0) \, , \end{aligned} \tag{A11}$$

where, as in (A10), we could restrict ourselves to initial and final channels, ν and ν', with identical J and π.

Equation (A11) can be further simplified by choosing the direction $\hat{\mathbf{k}}_0$ of the incident electron beam as quantization axes. We then find

$$Y_{\ell'}^{m^{\ell'}}(\hat{\mathbf{k}}_0) = \sqrt{\frac{2\ell' + 1}{4\pi}}\, \delta_{m^{\ell'}, 0} \quad ,$$

such that, due to (A9), the m^ℓ sum in (A11) disappears, and

$$m^{\ell} = m_0 - m + \underline{m}_0^j - \underline{m}^j \ .$$

With

$$Y_\ell^m(\theta,\varphi) = \Theta_\ell^m(\cos\theta)\, e^{im\varphi}$$

the θ and φ dependences can be separated and our final result for the jj-coupled amplitude, rewritten for convenient numerical implementation, is given by

$$f(\mathbf{k}\, m\, \underline{\gamma} \leftarrow \mathbf{k}_0\, m_0\, \underline{\gamma}_0) = \tilde{f}(\mathbf{k}\, m\, \underline{\gamma} \leftarrow \mathbf{k}_0\, m_0\, \underline{\gamma}_0)\, e^{im^{\ell}\varphi} \ ,$$

with

$$\begin{aligned}
&\tilde{f}(\mathbf{k}\, m\, \underline{\gamma} \leftarrow \mathbf{k}_0\, m_0\, \underline{\gamma}_0) \\
&= \left(\frac{\pi}{k_0 k}\right)^{1/2} i \sum_{\pi=\pm 1} \sum_{J=0}^{\infty} \sum_{j=|J-\underline{j}|}^{|J+\underline{j}|} \langle j\, m^j\, \underline{j}\, \underline{m}^j | J\, M\rangle \\
&\qquad \times \sum_{j'=|J-\underline{j}_0|}^{|J+\underline{j}_0|} \langle J\, M | j'\, m_0\, \underline{j}_0\, \underline{m}_0^j\rangle \\
&\qquad\quad \times \sum_{\ell=j-1/2}^{j+1/2} i^{-\ell}\, \delta_{\pi,\Pi(\ell,\underline{\ell})}\, \langle \ell\, m^{\ell}\, \tfrac{1}{2} m | j\, m^j\rangle\, \Theta_\ell^{m^{\ell}}(\cos\theta) \\
&\qquad\quad\quad \times \sum_{\ell'=j'-1/2}^{j'+1/2} i^{\ell'} \sqrt{2\ell'+1}\ \delta_{\pi,\Pi(\ell',\ell_0)}\, \langle j'\, m_0 | \ell'\, 0\tfrac{1}{2} m_0\rangle\, T_{\nu'\nu} \ . \qquad \text{(A12)}
\end{aligned}$$

In practice, the sum over J has to be truncated at a value $J_{\max}$ large enough to assure convergence of the quantity of interest derived from (A12).

---

* Present address: Department of Physics, Cardwell Hall, Manhattan, KS 66506-2601.
† Quantum Physics Division, National Institute of Standards and Technology, Boulder, CO.

[1] U. Thumm and D. W. Norcross, Phys. Rev. A **45**, 6349 (1992).
[2] J. C. Crown and A. Russek, Phys. Rev. **138**, A669 (1965).
[3] E. M. Karule, in *Atomic Collisions III*, edited by V. Ia. Veldre (Latvian Academy of Science, Riga, 1965); E. M. Karule and R. K. Peterkop, in *ibid.* (Latvian Academy of Science, Riga, 1965) (translations TT-66-12939 available through SLA Translation Center, John Crear Library, Chicago, IL).
[4] P. J. Visconti, J. A. Slevin, and K. Rubin, Phys. Rev. A **3**, 1310 (1971).
[5] E. Karule, J. Phys. B **5**, 2051 (1972).
[6] P. G. Burke and J. F. B. Mitchell, J. Phys. B **6**, L161 (1973).
[7] P. G. Burke and J. F. B. Mitchell, J. Phys. B **7**, 214 (1974).
[8] W. Gehenn and E. Reichert, J. Phys. B **10**, 3105 (1977).
[9] N. S. Scott, K. Bartschat, P. G. Burke, O. Nagy, and W. B. Eissner, J. Phys. B **17**, 3775 (1984).
[10] N. S. Scott, K. Bartschat, P. G. Burke, W. B. Eissner, and O. Nagy, J. Phys. B **17**, L191 (1984).
[11] B. Jaduszliwer and Y. C. Chan, Phys. Rev. A **45**, 197 (1992).
[12] U. Thumm and D. W. Norcross, Phys. Rev. Lett. **67**, 3495 (1991).
[13] I. I. Fabrikant, J. Phys. B **19**, 1527 (1986), and references therein.
[14] W. L. Nighan and A. J. Postma, Phys. Rev. A **6**, 2109 (1972).
[15] B. Stefanov, Phys. Rev. A **22**, 427 (1980).
[16] A. J. Postma, Physica **43**, 465 (1969).
[17] G. N. Hatsopoulos and E. P. Gyftopoulos, *Thermionic Energy Conversion* (MIT, Cambridge, MA, 1973), Vol. I; Vol. II (1979).
[18] H.-L. Zhou and D. W. Norcross, Phys. Rev. A **40**, 5048 (1989).
[19] J. M. Blatt and L. C. Biedenharn, Rev. Mod. Phys. **24**, 258 (1952).
[20] M. A. Morrison, Adv. At. Mol. Phys. **24**, 51 (1988).
[21] T. F. O'Malley, L. Spruch, and L. Rosenberg, J. Math. Phys. **2**, 491 (1961).
[22] K. Bartschat, Phys. Rep. **180**, 1 (1989).
[23] U. Thumm, K. Bartschat, and D. W. Norcross (unpublished).
[24] E. U. Condon and G. H. Shortley, *Theory of Atomic Spectra* (Cambridge University Press, Chicago, 1972).